Supporting Information:

Accelerated Particle-Based Target Capture – the Roles of Volume Transport and Near-Surface Alignment

Alexander van Reenen[1*], Arthur M. de Jong[1], and Menno W. J. Prins[1,2]

[1]Eindhoven University of Technology, Eindhoven, The Netherlands

[2]Philips Research, Eindhoven, The Netherlands

Document 1S Streptavidin loading on magnetic particles

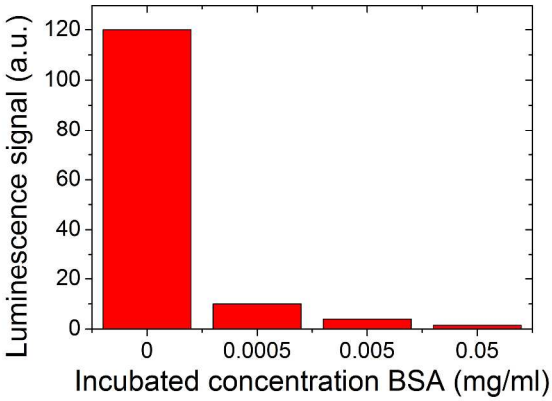

Figure 1S. Characterization of relative loading of streptavidin on magnetic particles using ELISA for different concentrations of BSA incubated in competition with streptavidin. In order to evaluate the loading, an excess of HRP (Horse-radish peroxidase) linked to biotin was incubated after functionalization. After washing unbound biotin-HRP away, luminol was added which exhibits chemiluminescence in the presence of HRP. The luminescence signal therefore is a measure for the amount of streptavidin on the particles.

Document 2S Losses in target concentration or reactive surface of capture particles

As discussed in the Theoretical Considerations section, Eq. 7 may only be applied to determine the reaction rate constant in case no significant depletion in reactants occurs. Here, the potential loss of reactants during the reaction is estimated.

The magnetic capture particles are completely covered with streptavidin, as specified by the manufacturer. Consequently, more than one target particle may bind to a capture particle, up to a maximum of ~800 target particles, in which case steric hindrance prohibits the binding of more target particles. In our experiments, due to the limited capture time which is considered, no more than 10 target particles are observed per capture particle. Taking into account only the top hemisphere of the target particles, this would correspond to a reduction of less than 3% in reactive surface of a capture particle, which is a negligible loss.

We can estimate the loss in target particle concentration, both for high and for low concentrations of capture particles. ~5×10^6 target particles are initially present in the sample fluid. For relatively low concentrations of capture particles (i.e. less than 4×10^3 MC in sample chamber), the maximum amount of bound targets per capture particle was ten FT for a time-span of 25 minutes. This corresponds to a loss in target concentration < 1 %, which has a negligible effect on the capture rate. For relatively high concentrations of capture particles, less than 300 bound targets are observed in a single field of view (containing at maximum ~2×10^3 capture particles). In total, at maximum ~3×10^5 capture particles are dispersed in the fluid chamber (0.5 μL of 7×10^8 MC/ml). From these numbers, it follows that ~ 1% of the target particles are captured after 25 minutes, which is negligible as well.

Based on these estimations, it is concluded that no significant losses in reactants occur in the considered time-span.

Document 3S Target capture at high surface coverages

Passive target capture by sedimented capture particles was studied at different capture particle concentrations. In Figure 2Sa, the amount of captured targets is shown in time for different capture particle concentrations, which is expressed in terms of the surface coverage. For low surface coverages, roughly linear behavior is observed. For surface coverages above 1%, clearly a non-linear increase in target capture is observed over time. This would also be expected, as for a complete surface coverage, the system acts as an absorbing plane, and as a result no steady-state solution can be obtained from the diffusion equation. Based on the diffusion equation, the captured amount should follow a $\sim t^{1/2}$ dependence. Therefore, we fitted the measured data with a function of the shape $y(t) = y_0 + \sqrt{(A(t-t_0))}$, in which A is a scaling parameter, and y_0 and t_0 are parameters which provide additional freedom concerning the offset of the curves. This was done since at $t = 0$ (closing of fluid chamber), not all particles might have sedimented yet, and the fluid containing the magnetic particles does not contain any target particles initially. Therefore the capture dynamics are likely to correspond to the fit function with a negative offset, both in time and captured amount of target. Note that without any such offsets, the fit-function would correspond to an initial concentration distribution which may be described (in terms of distance from the absorbing surface) as a step function, i.e. at $t = 0$, the target concentration at the absorbing surface is equal to the bulk concentration. In practice, this is not the case and therefore offsets are included in the fit function. As shown in Figure 2Sa, the data for higher surface coverage accurately fits a $t^{1/2}$ dependence. The fitted offset values are all negative ($t_0 \sim -100$ and $y_0 \sim -70$ with a variation of ~50%) as expected. From these results, it is concluded that for a relatively high coverage of the surface with capture particles, the capture process is similar to an absorbing plane, and as a consequence, no steady-state in the capture process is reached. The overall reaction rate constant is not constant and volume-transport becomes less efficient over time. To be able to compare target capture for varying surface coverage, we determined the average capture rates within the measured time-span of 25 minutes; see Figure 2Sb. It should be noted that Figure 2a may be obtained from Figure 2Sb using Eq. (7). Comparing the found capture rates, it is found that for a surface coverage below ~1%, the capture rate depends linearly on the number of particles

on the surface. For a higher surface coverage, it is found that the capture rate is roughly independent of the number of particles. This is in agreement with the previous conclusion that the surface acts as an absorbing plane for high surface coverage, i.e. target particle transport is not limited by finding a capture particle at the surface but rather by diffusive transport to reach the surface.

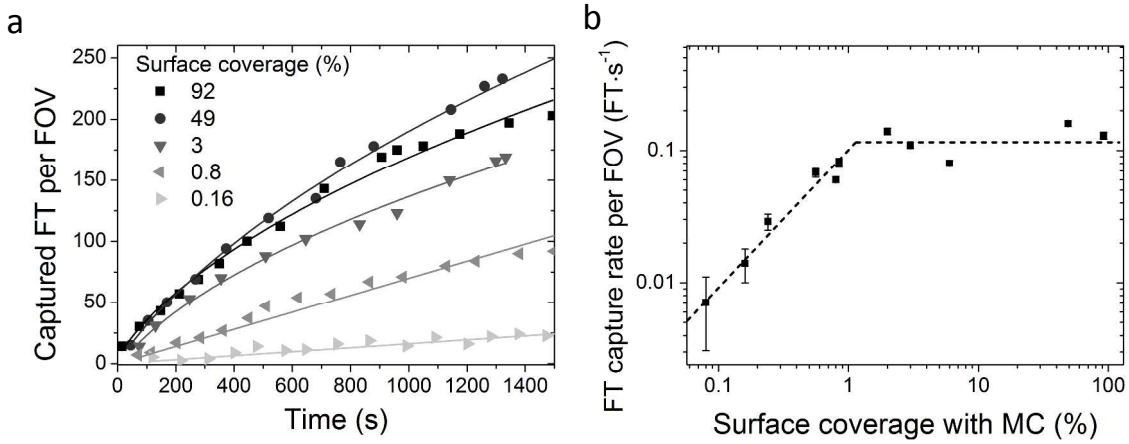

Figure 2S. Target capture at different surface coverage with capture particles. (a) Measured and fitted capture of fluorescent targets, as observed within a single field of view (FOV). For surface coverages > 1% the applied fit function is of the shape $y(t) = y_0 + \sqrt{(A(t-t_0))}$, with y_0, t_0 and A as fit parameters. For surface coverages < 1%, a linear fit is applied. (b) Determined average capture rates per field of view as obtained from linear fitting of the data in (a).

Document 4S Estimating DLVO interaction energies between target and capture particles

The interactions between charged surfaces within a liquid medium are described by the so-called DLVO theory developed by Derjaguin, Landau, Verwey and Overbeek. An overview of this theory for the field of biophysics has been given by Leckband and Israelachvili [19].

Here, we estimate the interaction energies of the electrostatic interaction as well as the Van der Waals interaction, for the case of two interacting spheres, with radius R_1 and R_2, corresponding respectively to the capture particle and the target particle.

First, the electrostatic (double-layer) interaction energy between two spheres, at a separation x, is given by

$$E_{es} = \frac{R_1 R_2}{R_1 + R_2} Z \exp(-\kappa x) \tag{1S}$$

In which κ is the inverse Debye length, which depends on the ionic strength of the liquid medium, and Z is the interaction potential[19], which depends on the surface potential ψ_0 of both surfaces and on the dielectric constant of the medium ε, i.e.

$$Z = 64\pi\varepsilon\varepsilon_0 \left(\frac{k_B T}{e}\right)^2 \tanh\left(\frac{ze\psi_{0,1}}{4k_B T}\right) \tanh\left(\frac{ze\psi_{0,2}}{4k_B T}\right) \tag{2S}$$

with z the valency of the electrolyte. As an approximation of the surface potential, we use the measured Zeta potential of the particles (see Experimental section). As the Zeta potentials of both target and capture particles are negative, the electrostatic interaction is repulsive, and will, if large enough, prevent the particles from coming into contact. We find that for a 0.18 M PBS solution, the electrostatic energy equals the thermal energy ($k_B T$) at an inter-particle distance of only ~3 nm, whereas for a 0.01 M (diluted) PBS solution, the thermal energy level is reached at ~ 13 nm.

In addition we can consider the Van der Waals interaction, which is given by

$$E_{es} = -\frac{A}{6x}\frac{R_1 R_2}{R_1 + R_2} \tag{3S}$$

with A the Hamaker constant, which, for interactions in a liquid medium such as water, is reported to be typically in the range of 0.5-1.5 $\times 10^{-20}$ J [19]. In Figure 3S, the total interaction energy (Van der Waals and electrostatic) is plotted for the cases of a 0.01 M and a 0.18 M PBS solution. For 0.18 M PBS no energy barrier is found that could prevent physical contact between the spheres, whereas for the 0.01 M PBS an energy barrier with a height of ~10 $k_B T$ is found. The energy barrier may explain why in 0.01 M PBS a strongly reduced target capture is observed.

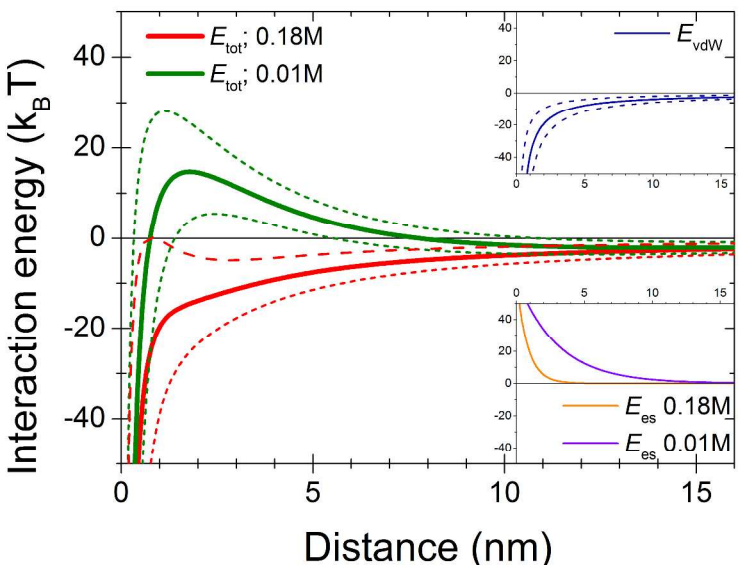

Figure 3S. Computed DLVO interaction energies for the interaction between two spherical particles (R_1 and R_2) in a liquid medium at $T = 293$ K. Dashed lines indicate error margins. The insets show separately the computed van der Waals and electrostatic interaction. Curves have been calculated for 0.01 M PBS and 0.18 M PBS. The energies are given in units of $k_B T$.

Document 5S Characterization of the response of magnetic particles in a rotating field

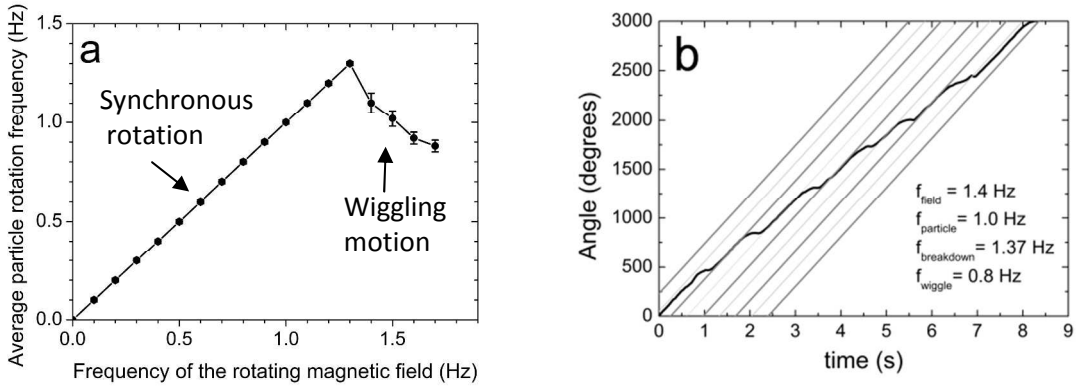

Figure 4S. Rotational response of an unbound magnetic particle on a glass surface in a rotating magnetic field (5 mT). This behavior is reported and described in more detail by van Reenen et al.[24] (see also [22]). (a) For low rotation frequencies of the magnetic field, the particle synchronously follows the field. Above a certain threshold frequency, called the breakdown frequency, the particle cannot follow the magnetic field anymore and assumes a wiggling motion. (b) Above the breakdown frequency, the particle exhibits a wiggling motion, i.e. it sometimes does and sometimes does not follow the field.

Document 6S Estimating radial transport due to rotation of a sphere in a viscous medium

The flow around a steadily rotating sphere in an infinite reservoir containing a non-compressible and homogeneous fluid has been studied extensively, both analytically and experimentally (see Fosdick et al. (1980)[23] for an overview). We consider in spherical coordinates (r,θ,φ) a sphere with radius $r = R$ that is rotating in the φ-direction with an angular velocity Ω. For this system, an analytical solution describing the steady flow field has been derived assuming no-slip conditions at the sphere boundaries. In our case, we are interested in the radial transport of fluid towards the rotating sphere, i.e.

$$u_{r,rot}(r,\theta) = -\frac{1}{2}\Omega^2\left(\frac{R^5}{4\nu r^2}\right)\left(1-\frac{R}{r}\right)^2\left(3\cos^2\theta - 1\right) \tag{4S}$$

with ν the kinematic viscosity (i.e. ~10^{-6} m^2/s for water at T = 293 K; ν equals the dynamic viscosity divided by the mass density of the fluid). Eq. 4S shows that there is an inward flow of fluid at the poles of the sphere ($\theta = 0°$) and an outward flow of fluid at the equator ($\theta = 90°$) due to centrifugal forces. The inward flow is maximal at $\theta = 0°$ and it is found to be maximal at a radial distance of $r = 2R$, e.g. taking $\Omega = 2\pi\cdot 10$ as an upper limit in our experiment: $u_{r,rot}$ $(2R,0) = -1.7 \times 10^{-10}$ m/s. Note that the minus-sign indicates that the fluid is moving towards the sphere. We can use u_r $(r,0)$ as an upper limit for the velocity at which target particles are transported towards the capture particle surface.

Now let us compare the rotation-induced with the concentration gradient-induced inward flow velocity of target particles. Using the analytical steady-state solution of the concentration profile, C^{ss} [see Figure 2b and Smoluchowski (1914)] and Fick's first law, we can determine the radial velocity of target particles:

$$u_{r,dif}(r) = \frac{J\big|_{r'=r}}{[FT]_{t=0}} = -D\frac{dC^{ss}}{dr'}\bigg|_{r'=r} = -D\frac{d\left(1-\frac{R}{r'}\right)}{dr'}\bigg|_{r'=r} = -D\frac{R}{r^2} \tag{5S}$$

Here J is the diffusion flux of targets. We find that the concentration gradient-induced flow velocity also depends on the radial coordinate; due to assumed symmetry it does not depend on θ or φ. Using Eq. 4S and 5S, we can determine the contribution of diffusive transport with respect to rotation-induced transport, as shown in Figure 5S. We find that for $r \to \infty$, diffusive transport is ~525 times larger than rotation induced transport (at 10 Hz rotation), whereas for short distances, this factor increases up to ~10^6.

As a consequence, radial transport induced by a 10 Hz rotation of a r = 1.4 μm sphere is negligible as compared to diffusive transport due to the concentration gradient. In our experiments, the nearby surface decreases diffusive transport, but only by a very small amount (~10%). The surface also slightly lowers the rotation-induced transport. So we conclude that in our experiments no measurable radial transport of targets is induced by the rotation of the magnetic particles.

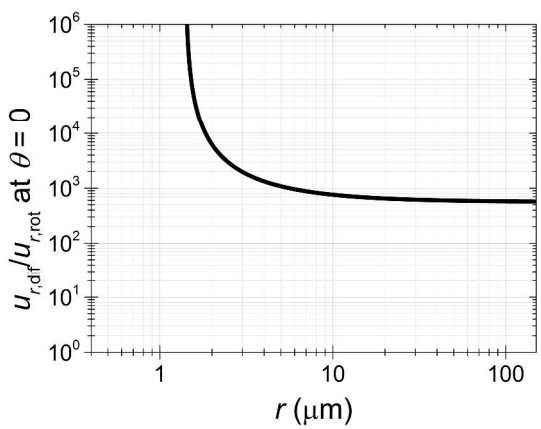

Figure 5S. Comparison between rotation-induced radial transport and diffusion-induced radial transport of targets. The curve corresponds to a rotation frequency of 10 Hz.

Document 7S Estimating the lifetime of an encounter complex

A good estimate of the lifetime of an encounter complex is the reciprocal of the rate constant which governs the separation of the encountered particles, i.e. $t_c \cong k_{sep}^{-1}$. In return, the separation rate constant may be obtained by estimating the equilibrium constant for complex formation K_{enc} (= k_{enc} / k_{sep}) and using the Smoluchowski equation, Eq. 3. An analytical equation for this equilibrium constant was found by Shoup et al.[25]. Based on classical statistical mechanics, they found analytically that the equilibrium constant for a spherically symmetric system without any additional interaction forces between the particles is simply equal to the reaction volume, i.e. the volume in which the binding reaction can occur. The system which we study here is indeed to a large extent spherically symmetric. Also, no significant interaction forces (typically electrostatic) are present at large distances due to the high ionic strength of the buffer solution (see Supporting Information 4S). Consequently, a good approximation of the encounter complex equilibrium constant may be obtained by calculating the reaction volume, which we estimate to be the whole volume of 5 up to 20 nm away from the capture particle: 0.12 μm^3 up to 0.5 μm^3 respectively. In other words, it is assumed that the particles have formed an encounter complex when distanced by 5 up to 20 nm. Using this estimation for the equilibrium constant K_{enc} and using $k_{enc} = k_{dif}$, we find that t_c ranges between 3 ms and 13 ms.

Document 8S Brownian rotation of a capture particle in an external magnetic field

In Eq. 10, it is assumed that the effect of the external magnetic field on the Brownian rotation of the capture particle is negligible. Here, we support this assumption by estimating the energy involved to rotate the ferromagnetic moment of the capture particle in a static magnetic field. It was reported by Janssen et al.[26] that the locked magnetic moment of the M270 magnetic particles equals $(1.3\pm0.4) \times 10^{-16}$ Am^2. In the presence of an external magnetic field (B = 5 mT), the magnetostatic energy is $U = \vec{m} \cdot \vec{B}$. Thus we find that an angular misalignment between the magnetic moment and the field of ~6° comes at a cost of about one times $k_B T$. Now let us compare this angle to the root-mean-square rotation angle of the capture particle after 0.01 seconds, which is the typical encounter complex lifetime as estimated in Document 7S. Using $\theta_{rms} = (2D_{rot,MC} \cdot t)^{0.5}$, we find a root-mean-square rotation of $\theta_{rms} \cong 2°$. This angle is small and involves a magnetostatic energy of only 0.1 $k_B T$. So we conclude that the presence of an external field of 5 mT negligibly affects the Brownian rotation of the magnetic capture particle.

Moreover, we have numerically computed the angular excursion of a magnetic particle for the following three cases: (i) no external magnetic field, (ii) a static magnetic field of 5 mT and (iii) a magnetic field of 5 mT that rotates at 1 Hz. Brownian rotation was included following the numerical scheme as described and verified by Grassia et al[27], which defines an effective Brownian motion torque, τ_{random}. The angular excursion was computed using a forward Euler method with timesteps of Δt = 0.1 ms:

$$\theta_{i+1} = \theta_i + \Delta t \cdot \left[\frac{mB\sin(\omega t - \theta_i) + \tau_{random}}{8\pi\eta C R_{MC}^3} \right] \tag{6S}$$

Here $C \cong 1.2$ is a correction factor to account for the additional viscous drag[25] on the particle due to the nearby physical surface.

In Figure 6Sa the angular excursions are plotted for the three different cases. From the computed data, the angular difference in excursion over 0.01 s (~encounter lifetime) was determined, as shown in Figure 6Sb

and Figure 6Sc. Comparing cases (i) and (ii), i.e. the absence and presence of a static field, no significant differences are found. A static magnetic field of 5 mT causes a reduction of the root-mean-square angular rotation of ~3%. Also compared to a rotating magnetic field (1 Hz and 5 mT), no significant deviation is found in the root-mean-square rotation, other than the mean excursion which is clearly non-zero due to the forced particle rotation.

Based on these results, we conclude that an external magnetic field of 5 mT has a negligible effect on the Brownian rotation of the capture particle.

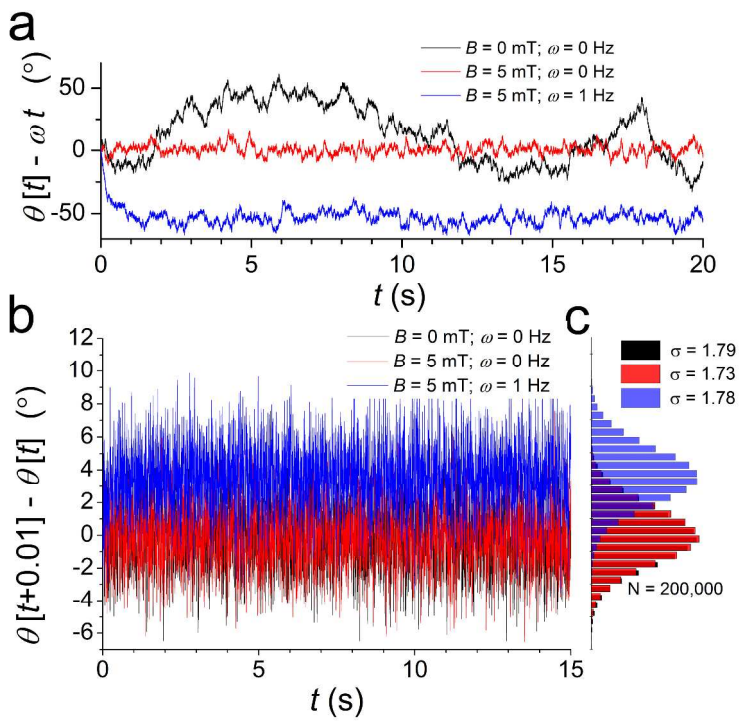

Figure 6S. Simulation of angular excursion of a capture particle in the absence or presence of a static or rotating external magnetic field. (a) Computed excursion with respect to the magnetic field direction for the different cases. (b) Processed data from the angular excursion: the angular difference in excursion over 0.01 s, i.e. the estimated lifetime of the encounter complex. (c) Histograms corresponding to the data in (b). The determined standard deviation is shown in the figure. Note that the data corresponding to an absent external magnetic field (black curves in (b) or bars in (c)) falls for a large part behind the data corresponding to a static magnetic field (red curves and bars).

Supporting references

(24) van Reenen, A.; Gutierez, F.; van Ijzendoorn, L. J.; Prins, M. W. J. *Biophysical Journal*, *submitted*

(25) Shoup, D.; Szabo, A. *Biophysical Journal* **1982**, *40*, 33-39.

(26) Janssen, X. J. A.; van Noorloos, J. M.; Jacob, A.; van IJzendoorn, L. J.; De Jong, A. M.; Prins, M. W. J. *Biophysical Journal* **2011**, *100*, 2261-2267.

(27) Grassia, P. S.; Hinch, E. J.; Nitsche, L. C. *Journal of Fluid Mechanics* **1995**, *282*, 373-403.